

## Structure of the Resonance Attractor for Spiral Waves in Excitable Media

A. Karma<sup>1</sup> and V. S. Zykov<sup>2</sup>

<sup>1</sup>*Department of Physics and Center for Interdisciplinary Research on Complex Systems,  
Northeastern University, Boston, Massachusetts 02115*

<sup>2</sup>*Otto-von-Guericke-Universität, Universitätsplatz 2,  
D-39106 Magdeburg, Germany*

(Received 11 May 1999)

Recent experiments in the light-sensitive Belousov-Zhabotinsky reaction have shown that a pulsatory modulation of excitability controlled by a feedback can force the spiral wave core to execute a circular trajectory around a fixed measuring point of the medium. A theory is developed to explain the existence and stability of this resonance attractor which is based on reducing the spiral wave dynamics to a low-dimensional map. The analysis of this map predicts the existence of a discrete set of stable circular trajectories in good quantitative agreement with numerical simulations of the two-component Oregonator model. Only a small part of this set has so far been observed experimentally.

PACS numbers: 82.40.Bj, 05.45.Ac, 47.54.+r, 82.20.Wt

Spiral waves are ubiquitous structures in reaction-diffusion systems of both physical and biological origin [1–3]. These waves typically rotate rigidly or meander around a central core region and their dynamics becomes even richer if the medium undergoes an external forcing. A spatially uniform periodic forcing results in an entrainment of spiral waves [4,5] or in a resonance drift of the core predicted theoretically [6] and observed recently in experiments with the light-sensitive Belousov-Zhabotinsky (BZ) reaction [7]. Numerical simulations [8] and theoretical analysis [9] have confirmed that the properties of the resonant drift for rigidly rotating and for meandering spiral waves are very similar. The phenomenon of resonant drift is of interest because it provides a direct means to *control* spiral motion, and may have interesting applications such as to defibrillate cardiac tissue by pushing out this undesirable source of excitation [10]. Implementing control, however, generally requires some form of feedback since the basic spiral rotation period and location are not usually known beforehand.

One of the simplest feedback schemes consists of measuring the activity level at a particular point of the system and applying a brief spatially uniform pulsatory modulation at a fixed time delay  $\tau$  after the passage of a wave front at this point [11]. As demonstrated in the light-sensitive BZ reaction, the measuring point imposes a center of symmetry for the dynamics and the resonant drift results in a clocklike motion of the spiral wave core along a circular pathway around this center [7,11]. Moreover, it was shown that the size of this *resonance attractor* can be changed by varying the parameters of the feedback loop [7,11]. It is clear also that this size should depend on the parameters of the medium [12].

In this Letter, we develop a simple theory that allows us to explain the generic features of this resonance attractor, and we validate its predictions by numerical simulations of the two-variable Oregonator model. The main idea is to describe the dynamics of the spiral wave core in terms

of an iterative map that gives the new location of the core after each applied pulse.

In view of the experimental motivation, we examine a light-sensitive excitable media like the ruthenium-catalyzed BZ reaction. Wave propagation in this medium can be simulated by the Oregonator model [13,14] with an additional term  $\phi(t) = \phi_0 + I(t)$  describing the effects of an external illumination [4,8]:

$$\begin{aligned} \frac{\partial u}{\partial t} &= \nabla^2 u + \frac{1}{\epsilon} \left[ u - u^2 - (fv + \phi) \frac{u - q}{u + q} \right], \\ \frac{\partial v}{\partial t} &= u - v. \end{aligned} \quad (1)$$

The variables  $u$  and  $v$  describe the concentrations of the autocatalytic species  $\text{HBrO}_2$  and the catalyst, respectively. The parameters  $\epsilon = 0.05$ ,  $q = 0.002$ ,  $f = 3.5$ , and  $\phi_0 = 0.01$  are fixed.

Under these parameters the spiral wave [i.e., a region where  $u(x, y, t) > 0.1$ ] rotates rigidly with the period  $T_0 = 6.85$  around a circular core as shown in Fig. 1 [15]. The thick (thin) solid lines show the front (back) of the wave, where  $\partial u / \partial t > 0$  ( $\partial u / \partial t < 0$ ). By definition the spiral wave tip is a point on the contour line, where  $\partial u / \partial t = 0$ . The trajectory of the spiral tip describes the boundary of the spiral core. The radius of the core increases when the intensity  $\phi_0$  of a stationary and spatially homogeneous illumination is increased [5,8]. Thus, the application of a short impulse of the illumination results in a sudden shift of the spiral core. The spiral wave core dynamics is then the sequence of these shifts under a sequence of such impulses.

The feedback algorithm implies that illumination impulse  $I(t)$  should be generated each time that the wave front passes through a particular measuring point [11]. Our aim is to describe the displacement of the spiral wave core under such an external forcing. We measure the position of the core center in a polar coordinate system  $(R, \varphi)$  with the origin at the measuring point (see Fig. 1).

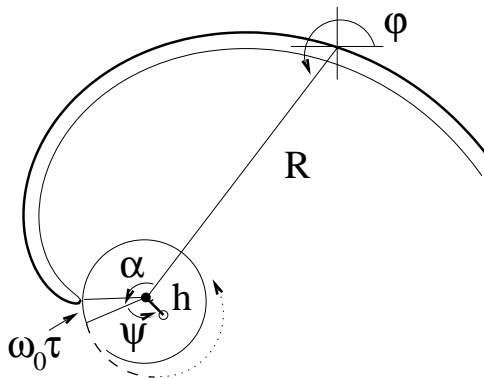


FIG. 1. A spiral wave rotating around a circular core is shown at the time when the wave front (thick solid line) passes through the measuring point (thin cross). The application of an illumination impulse induces a shift of the spiral core center (filled circle) to the new position (open circle) resulting in a shifted steady-state circular trajectory of the spiral tip (dotted curve). The trajectory of the spiral wave during some intermediate process is shown by a dashed curve.

The angle  $\alpha$  describes rotation around the spiral wave core. This angle is measured from the line connecting the core center and the measuring point. The shape of the spiral front can be given by a function  $\Theta(r)$ , where  $(r, \Theta)$  is the polar coordinate system with the origin at the core center. Thus, the equation  $\alpha = -\Theta(R)$  is valid at the instant when the wave front traverses the measuring point. An illumination impulse with a duration  $D$  and an amplitude  $A$  is generated after the time delay  $\tau$ . Let  $\alpha_i, R_i,$  and  $\varphi_i$  denote the value of these variables evaluated at the time  $t_i$  at which the  $i$ th external impulse is applied. By the use of purely geometrical consideration (see Fig. 1), it is straightforward to derive the following map to describe the motion of the core center:

$$\alpha_i = \omega_0\tau - \Theta(R_i), \tag{2}$$

$$R_{i+1}^2 = R_i^2 + h^2 - 2R_i h \cos(\psi + \alpha_i), \tag{3}$$

$$\varphi_{i+1} = \varphi_i - \arcsin[(h/R_{i+1}) \sin(\psi + \alpha_i)], \tag{4}$$

where  $h$  and  $\psi$  denote, respectively, the absolute value and the angular direction of the shift of the spiral core due to one light impulse. Note that the above map is effectively only two dimensional because  $\phi_i$  does not enter on the right-hand sides of (2) and (3). In general,  $h$  and  $\psi$  can be measured experimentally or determined by numerical integration of the reaction-diffusion equations. Here, the integration of the model (1) yields the values  $h = 1.75$  and  $\psi = 1.446$  for a single impulse with  $D = 0.3$  and  $A = 0.004$ . For an impulse of the same duration but of a negative amplitude  $A = -0.004$ , we obtained  $h = 2.346$  and  $\psi = -1.226$ .

The function  $\Theta(r)$  resulting from an integration of the Oregonator model (1) is plotted in Fig. 2 by a solid line. The radius  $r_q$  represents the shortest distance between

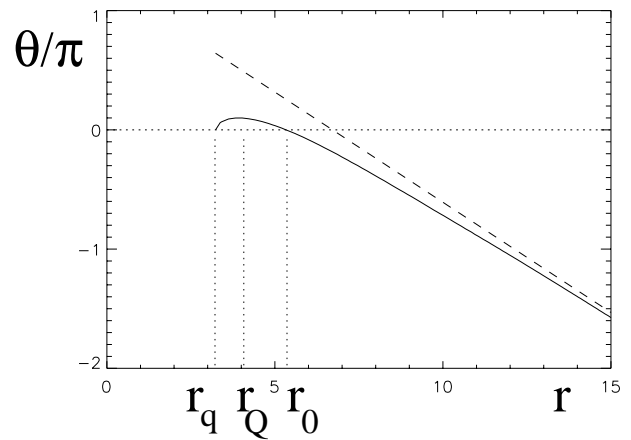


FIG. 2. Function  $\Theta(r)$  (solid line) obtained for a spiral wave in the Oregonator model (1). The dashed line represents the asymptotic behavior of  $\Theta(r)$  for  $r \rightarrow \infty$ .

the spiral wave and the core center and corresponds to the trajectory of the spiral tip. At this point the radial direction from the core center is orthogonal to the front. The function  $\Theta(r)$  increases with  $r$  in a vicinity of  $r_q$ , reaches a maximum value at  $r = r_Q$ , and then starts to decrease and becomes negative for  $r > r_0$ . The dashed line in Fig. 2 represents the asymptotic behavior for  $r \rightarrow \infty$ . This asymptote was identified as  $\Theta = \Theta_0 - 2\pi r/\lambda$ , where  $\Theta_0 = 1.2$  and  $\lambda = 34.5$ . As is well known, far away from the core center, the shape of the wave front can be described by an Archimedean spiral with a pitch  $\lambda$ . Near the core, however, the shape of the front deviates considerably from an Archimedean spiral, and  $\Theta(r)$  becomes a nonmonotonous function (see Fig. 2), as described analytically in the large core limit [16].

Let us start by analyzing the system (2)–(4) under the assumptions  $h/R_i \ll 1$  and  $|\psi| - \pi/2 \ll 1$ , which become accurate in the limit of a small amplitude and short impulse. In this case, Eqs. (3) and (4) become

$$R_{i+1} = R_i + h \sin(\psi) \sin(\alpha_i), \tag{5}$$

$$\varphi_{i+1} = \varphi_i - h \sin(\psi) \cos(\alpha_i)/R_{i+1}. \tag{6}$$

The two-dimensional map defined by (2) and (5) has a discrete spectrum of fixed points described by

$$R_s = \Theta^{-1}(\omega_0\tau - k\pi), \tag{7}$$

$$\alpha_s = k\pi, \quad k = 0, 1, 2, \dots \tag{8}$$

These fixed points correspond to steady-state circular trajectories of the core of radius  $R_s$  around the measuring point, where  $R_s$  can take on a discrete set of values. Several curves  $R_s = R_s(\tau)$  corresponding to different  $k$  in (7) are plotted in Fig. 3(a) using the function  $\Theta(r)$  shown in Fig. 2. Note that the function  $\Theta(r)$  becomes linear for large  $r$  (see Fig. 2). In this limit Eqs. (7) and (8) should describe an equidistant spectrum of fixed points with a

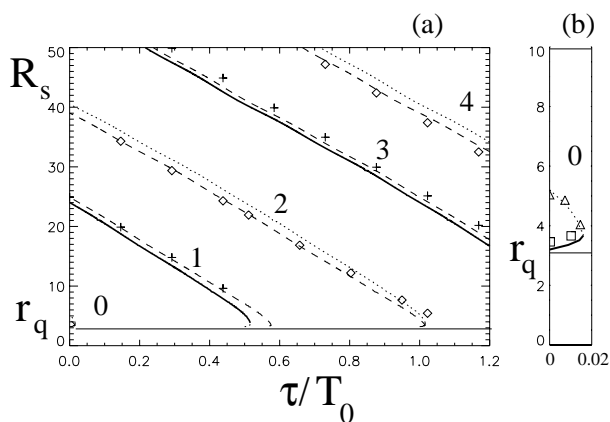


FIG. 3. (a) Structure of the resonance attractor for  $\psi > 0$ . The radius  $R_s$  of stable attractors (solid curves) and the unstable separatrix (dotted curves) are plotted as a function of the time delay  $\tau$ . The dashed curves correspond to the improved prediction of Eq. (10) and the thin solid line indicates the smallest possible size of the resonance attractor. (b) Magnification of (a) near the origin by the use of a different scale.

spacing  $\lambda/2$ , as was mentioned in [12]. However, this linear approximation completely fails for  $R_s \approx R_Q$  where the function  $\Theta(r)$  is essentially nonlinear. In particular, a magnified plot of the attractor with  $k = 0$  is shown in Fig. 3(b) by use of another scale.

Linearization of (2) and (5) around the fixed points yields at once the stability condition

$$-h \cos(k\pi) \sin(\psi) \left. \frac{d\Theta}{dR} \right|_{R_s} < 0, \quad (9)$$

for the attractor of radius  $R_s$ . Let us first examine the implication of this stability condition for the case  $\psi > 0$ . In this case, one part of each curve in Fig. 3 with  $R_s > r_Q$  is associated with a negative slope  $d\Theta/dR$ . This part therefore corresponds to a stable motion for any odd  $k$ . The other part with  $R_s < r_Q$  corresponds to a positive slope  $d\Theta/dR$  and is stable for any even  $k$ . All stable (unstable) steady states of the system (2) and (5) are shown as solid (dotted) lines in Fig. 3. For  $\psi < 0$ , the opposite situation is true and all dotted (solid) lines in Fig. 3 correspond to stable (unstable) attractors. It is important to stress that the dotted (solid) line corresponding to a given unstable steady-state  $k$  for  $\psi > 0$  ( $\psi < 0$ ) plays the role of a separatrix between the basins of attraction of the stable attractors  $k - 1$  and  $k + 1$ . Thus, the set of these separatrices determines which attractor is selected from an arbitrary initial condition. Finally, the thin horizontal line in Fig. 3 corresponds to  $R_s = r_q$ . If the distance between the spiral core center and the measuring point is smaller than  $r_q$ , the wave front never traverses the measuring point and no light impulse is generated. Thus, in this case, the attractor is simply the unperturbed rigid rotation of the spiral wave around a circular core.

To test these predictions we have computed the size of the resonance attractor by simulating (1) using positive (negative) impulses  $I(t)$ . The results of these computations for  $A = 0.004$  ( $A = -0.004$ ) with the duration of the light impulses  $D = 0.3$  are shown in Fig. 3 as crosses (diamond). The simulation data are located very close to the solid or dotted lines predicted by the map defined by (2) and (5). The small systematic error (about 5%) can be corrected by using the original map (2) and (3) instead of the approximation (2) and (5). Indeed, the analysis of this map yields, instead of (7), the predictions

$$\omega_0 \tau = \Theta(R_s) \pm \arccos[h/(2R_s)] - \psi + 2m\pi. \quad (10)$$

Several stable branches corresponding to (10) are plotted as dashed lines in Fig. 3. This more precise estimate shows that, for a given  $\tau$ , the size of the attractor becomes larger (smaller) with respect to the prediction of (7) for a positive (negative) impulse.

Decreasing  $D$  leads to a better agreement with the estimate (7). Results of such computations performed for  $D = 0.1$  and  $A = 0.003$  ( $A = -0.003$ ) are shown by triangles (squares) in Fig. 3(b). A single positive (negative) impulse for these parameters yields a shift of the spiral core  $h = 0.49$  and  $\psi = 1.52$  ( $h = 0.46$  and  $\psi = -1.39$ ), where  $\psi$  is closer to the limiting value  $|\psi| = \pi/2$  assumed in the derivation of (5) and (6).

Figures 4 and 5 illustrate that the iteration of the map (2)–(4) predicts accurately the core evolution simulated in the reaction-diffusion model (1) from an arbitrary initial condition. In the example of Fig. 4(a) corresponding to  $\tau = 0$  and  $\psi > 0$ , the initial distance between the spiral core center and the measuring point,  $R_0 = 5.5$ , is below the solid line (1) in Fig. 3(a) [ $R_s(0) = 24$  for  $k = 1$ ] but above the dotted line (0) [ $R_s(0) = 5.2$  for  $k = 0$ ]. In Fig. 4(b), the initial distance  $R_0 = 39.0$  is above the solid line (1) in Fig. 3(a) but below the dotted line (2). Thus, according to the predictions of the map, the same attractor  $R_s(0) = 24$  should be selected in both cases in agreement with the simulation results.

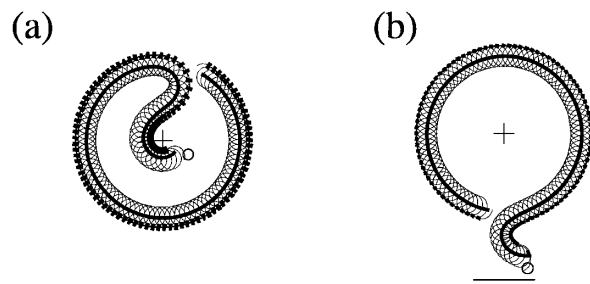


FIG. 4. Trajectories of the spiral wave tip (thin solid line) computed with the Oregonator model (1) for  $\tau = 0$ ,  $A = 0.004$ , and  $D = 0.3$ . Thick segments correspond to the application of impulses. The core trajectories predicted by the map (2)–(4) (thick solid lines) are in excellent agreement. The small open circles indicate the initial location of the spiral wave tip. Scale bar: 20. (a) and (b) correspond to different initial conditions (see text).

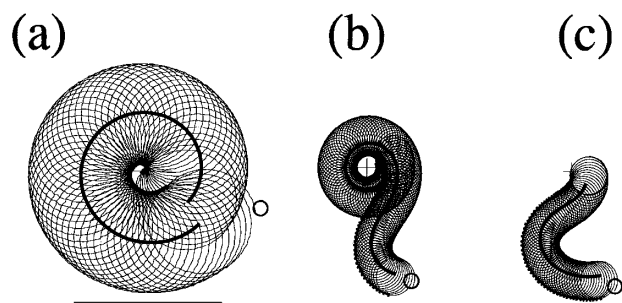


FIG. 5. Tip trajectories in the Oregonator model and core trajectories predicted by the map (2)–(4) for  $\tau = 0$ ,  $A = 0.003$  (a);  $\tau = 0$ ,  $A = -0.003$  (b); and  $\tau = 0.5$ ,  $A = -0.003$  (c). The impulse duration is  $D = 0.1$ . Scale bar: 10.

In Fig. 5(a), a trajectory with  $\tau = 0$  and a positive impulse is shown which corresponds to the smallest possible size of the resonance attractor  $R_s = r_q$ . In order to reach this attractor,  $R_0$  was chosen within the interval  $r_q < R_0 < r_0$ . A small increase of  $R_0$  results in the trajectory shown in Fig. 4(a). This correlates perfectly with Fig. 3(b) because a separatrix (dotted line for  $k = 0$ ) is located quite close to this attractor. Next, this separatrix transforms into a stable attractor if a negative impulse is chosen [Fig. 5(b)]. In contrast to the previous case, the basin of attraction for this attractor is relatively large [between  $r_q$  and  $R_s = 24$  corresponding to the solid curve (1) in Fig. 3(a)]. For this reason, the attractor was reached even though the initial distance was rather large ( $R_0 = 19.7$ ). Finally, increasing  $\tau$  up to  $\tau = 0.5$  results in the trajectory shown in Fig. 5(c). In agreement with Fig. 3, the spiral wave core starts to drift towards the measuring point thereby decreasing the distance between the spiral wave core and the measuring point. For this time delay ( $\tau/T_0 = 0.07$ ), however, there are no attractors with a radius smaller than the initial distance  $R_0 = 19.7$ . As a result the drift stops when the distance becomes shorter than  $r_q$  (thin solid line in Fig. 3). In this final regime the measuring point is located inside the spiral wave core and light impulses are no longer generated.

In summary, the simulations perfectly confirm the basic structure of the resonance attractor displayed in Fig. 3. The map (2)–(4) allows one to predict the possible sizes of the resonance attractor for a given time delay  $\tau$  and the core dynamics from an arbitrary initial condition as illustrated by Figs. 4 and 5. Here, we have developed this theory for rigid rotation of the unperturbed state and under the assumption that all relaxation processes after the light impulse is switched off occur on a time scale smaller than the basic spiral period  $T_0$ . The extension of this theory

to include meander and longer time memory effects is an interesting problem for future studies.

The theory elaborated in this Letter produces a clear explanation of the experimental observation of a resonance attractor under a pulsatory modulation of the medium excitability controlled by a feedback [7,11]. In particular, the dependence  $R_s(\tau)$  observed in [7] can be interpreted as one of a discrete set of stable branches shown in Fig. 3. Thus, the complex structure of the resonance attractor elucidated here analytically and numerically should stimulate future experimental studies in order to discover the other predicted stable branches, not yet observed. Moreover, the strategy of reducing the spiral wave dynamics to a low dimensional map that describes the core evolution should prove useful in a wide range of control applications.

One of us (A. K.) thanks the American Heart Association for support.

- [1] A. T. Winfree, *When Time Breaks Down* (Princeton University Press, Princeton, 1987).
- [2] *Spatio-Temporal Organization in Nonequilibrium Systems*, edited by S. C. Müller and Th. Plesser (Projekt Verlag, Dortmund, 1992).
- [3] *Chemical Waves and Patterns*, edited by R. Kapral and K. Showalter (Kluwer, Dordrecht, 1995).
- [4] O. Steinbock, V. S. Zykov, and S. C. Müller, *Nature* (London) **366**, 322 (1993).
- [5] M. Braune and H. Engel, *Chem. Phys. Lett.* **211**, 534 (1993).
- [6] V. A. Davydov, V. S. Zykov, A. S. Mikhailov, and P. K. Brazhnik, *Radiophys. Quantum Electron.* **31**, 574 (1988).
- [7] S. Grill, V. S. Zykov, and S. C. Müller, *J. Phys. Chem.* **100**, 19082 (1996).
- [8] V. S. Zykov, O. Steinbock, and S. C. Müller, *Chaos* **4**, 509 (1994).
- [9] R. M. Mantel and D. Barkly, *Phys. Rev. E* **54**, 4791 (1996).
- [10] V. N. Biktashev and A. V. Holden, *Phys. Lett. A* **181**, 216 (1993); *Chaos Solitons Fractals* **5**, 575 (1995).
- [11] S. Grill, V. S. Zykov, and S. C. Müller, *Phys. Rev. Lett.* **75**, 3368 (1995).
- [12] E. N. Nikolaev, V. N. Biktashev, and A. V. Holden, *Chaos Solitons Fractals* **9**, 363 (1998).
- [13] R. Field and R. Noyes, *J. Chem. Phys.* **60**, 1877 (1974).
- [14] J. J. Tyson, in *Oscillations and Travelling Waves in Chemical Systems*, edited by R. Field and M. Burger (Wiley, New York, 1985), p. 93.
- [15] The computations were performed by an explicit Euler method using a five-point finite-difference representation of the Laplacian on a  $600 \times 600$  lattice with a grid spacing  $\Delta x = \Delta y = 0.2$  and a time step  $\Delta t = 0.002$ .
- [16] V. Hakim and A. Karma, *Phys. Rev. Lett.* **79**, 665 (1997); e-print cond-mat/9903262, 1999.